HHS Public Access

Author manuscript

Magn Reson Med. Author manuscript; available in PMC 2017 June 01.

Published in final edited form as:

Magn Reson Med. 2016 June ; 75(6): 2442–2447. doi:10.1002/mrm.25821.

O_2-Sensitive MRI Distinguishes Brain Tumor *vs*. Radiation Necrosis in Murine Models

Scott C. Beeman[1], **Ying-Bo Shui**[2], **Carlos J. Perez-Torres**[1], **John A. Engelbach**[1], **Joseph J.H. Ackerman**[1,3,4,5], and **Joel R. Garbow**[1,5]

[1]Department of Radiology, Washington University, St. Louis, MO

[2]Department of Ophthalmology, Washington University, St. Louis, MO

[3]Department of Chemistry, Washington University, St. Louis, MO

[4]Department of Internal Medicine, Washington University, St. Louis, MO

[5]Department of Alvin J. Siteman Cancer Center, Washington University, St. Louis, MO

Abstract

Purpose—To quantify the relationship between ^{1}H longitudinal relaxation rate constant, R_1, and O_2 concentration (relaxivity, r_1) in tissue and to quantify O_2-driven changes in R_1 (ΔR_1) during a breathing gas challenge in normal brain, radiation-induced lesions, and tumor lesions.

Methods—Relaxivity determination. R_1 data were collected in control-state mice (n=4) during three different breathing gas (and thus tissue O_2) conditions. In parallel experiments, pO_2 was measured in the thalamus of control-state mice (n=4) under the same breathing gas conditions using an O_2-sensitive micro-probe. The relaxivity of tissue O_2 was calculated using the R_1 and pO_2 data.

Pathology determination. R_1 data were collected in control-state (n=4) mice, a glioma model (n=7), and a radiation necrosis model (n=6) during two breathing gas (thus tissue O_2) conditions. R_1 and ΔR_1 were calculated for each cohort.

Results—O_2 r_1 in the brain was $9\times10^{-4}\pm3\times10^{-4}$ $mmHg^{-1}s^{-1}$ at 4.7T. R_1 and ΔR_1 measurements distinguished radiation necrosis from tumor ($p<0.03$ and $p<0.01$, respectively).

Conclusion—The relaxivity of O_2 in brain is determined. R_1 and ΔR_1 measurements differentiate tumor lesions from radiation necrosis lesions in the mouse models. These pathologies are difficult to distinguish by traditional imaging techniques; O_2-driven changes in R_1 holds promise in this regard.

Keywords

tissue oxygenation; T_1 Relaxometry; Radiation Necrosis; Tumor

*Corresponding Author: Joel R Garbow, Biomedical MR Laboratory, Campus Box 8227, Washington University School of Medicine, Room 2313, 4525 Scott Ave, St Louis, MO 63110, USA, Fax: +1 314 362 0526, Phone: +1 314 362 9949, garbow@wustl.edu.

INTRODUCTION

Diatomic (molecular) oxygen (O_2), as found dissolved in tissue, is a critical component in aerobic metabolism and is, thus, a fundamental determinant of physiologic functional status. Quantitative mapping (imaging) of tissue oxygenation is a developing field that holds much promise for informing on perfusion and metabolism in healthy tissue and a variety of pathologies including stroke, diabetes, and cancer (1–10). Well-developed techniques like positron emission tomography (PET) (11–13) and quantitative blood-oxygen level dependent (qBOLD) magnetic resonance imaging (MRI) (14–20) have been implemented as surrogate markers of tissue O_2 content. PET tracers have been synthesized that locate in (and thus identify) hypoxic cells and qBOLD MRI can be used to infer oxygen extraction fraction from magnetic susceptibility changes in the surrounding vasculature. However, these methods have yet to receive widespread adoption. PET is challenged by modest spatial resolution, exposure to radioactive tracers, and often prohibitive infrastructure requirements. qBOLD MRI generally requires high magnetic field homogeneity, a challenge near boundaries of tissue differing in magnetic susceptibility (21).

Alternatively, it has long been recognized that O_2 is weakly paramagnetic and therefore influences (increases) the ^1H longitudinal ("spin-lattice") relaxation rate constant (R_1) of tissue water as measured by NMR/MRI. As with any relaxation agent at low concentration, the effect is, in principle, linearly proportional to oxygen concentration (22,23), Eq. [1],

$$R_1 = R_{1,0} + r_1 \times pO_2, \quad [1]$$

where R_1 is the longitudinal (z-axis) relaxation rate constant (sec^{-1}), which is typically determined by MRI on a voxel-by-voxel basis, $R_{1,0}$ is the (background) tissue relaxation rate constant (sec^{-1}) in the absence of O_2, pO_2 is partial pressure of oxygen (mmHg) dissolved in the tissue water, and r_1 is the relaxivity of O_2 ($mmHg^{-1}\ sec^{-1}$ or, equivalently, $mM^{-1}\ sec^{-1}$). This expression can also be written in terms of the molar concentration of O_2, $[O_2]$. O_2 relaxivity depends on the correlation time for the dipolar interaction between the paramagnetic O_2 molecule and the ^1H spins of water, and on magnetic-field strength (i.e., on the spectral density at the resonance frequency). Reports of O_2 relaxivity are sparse: 2.5×10^{-4} $mmHg^{-1}\ sec^{-1}$ in plasma at 8.5T (24), 2.7×10^{-4} $mmHg^{-1}\ sec^{-1}$ in cerebrospinal fluid at 1.5T (25), 2.0×10^{-4} $mmHg^{-1}\ sec^{-1}$ (26) and 2.2×10^{-4} $mmHg^{-1}\ sec^{-1}$ (27) in saline phantoms at 4.7T, and 4.2×10^{-4} $mmHg^{-1}\ sec^{-1}$ in water at 0.5T (28).

In principle, it is straightforward to create a map of tissue pO_2 (or $[O_2]$) from a MRI map of R_1. In practice, however, there are significant challenges to deriving absolute tissue pO_2 values, due largely to the low relaxivity of O_2. For example, blood flow can contribute to recovery of tissue water ^1H longitudinal magnetization, masking the contribution of dissolved O_2 to the overall relaxation process. Nevertheless, oxygen-*sensitive* MRI experiments, coupled with breathing-gas modulation, have been used to non-invasively interrogate tissue oxygenation in tumor (2,3,8,27), radiation treatment (29), and a number of control-state (normal, healthy) organs (1,5,7,30).

Quantification of tissue oxygenation is particularly valuable for detecting and characterizing pathologies that involve metabolic changes such as cancer (31), diabetes, metabolic

syndrome, and infection. Recently, our group has developed a murine model of single-hemisphere, late-onset radiation necrosis (32,33), a pathology that occurs in up to 23% of radiation-treated brain-tumor patients (34). Late-onset radiation necrosis is a particularly challenging pathology, as it is indistinguishable from recurrent tumor when viewed with common radiological techniques. Because the metabolic states of late-onset radiation necrosis and recurrent tumor are quite different, we hypothesize that an oxygen-sensitive MRI technique will distinguish these pathologies, an advance that would inform subsequent treatment plans.

The goals of this work are two-fold: (i) Quantify the relationship between ^{1}H longitudinal relaxation rate constant, R_1, and O_2 concentration (relaxivity, r_1) in tissue and (ii) Demonstrate that MRI-measured tissue oxygenation changes can differentiate radiation-induced lesions from brain tumors.

METHODS

Correlation of R_1 and brain tissue [O_2]: control-state (baseline)

All animal experiments were approved by the Washington University Division of Comparative Medicine. The effects of breathing gas composition on brain-tissue-water R_1 were quantified *in vivo* in control-state (normal, healthy) nine-week-old female BALB/c mice (Harlan Laboratories, Indianapolis, IN) anesthetized with 0.8% isoflurane. R_1 data were collected (see *MRI methods*) during alternate free breathing of pure oxygen, a hypoxic gas mixture (12.5% O_2 / 87.5% N_2), and carbogen (95% O_2/5% CO_2). One R_1 dataset was collected for each of the three breathing gas compositions in each animal (n = 4). R_1 data were collected 20 minutes after the start of free breathing of each gas composition to allow tissue oxygen levels to equilibrate. The order in which the breathing gas compositions were administered was randomized amongst animals.

The relationship between R_1 and pO_2 of brain tissue *in vivo*, and thus the *in vivo* relaxivity of O_2, was established using an oxygen sensitive optical micro-probe (Oxford Optronix, Abington, OX, UK). Optical pO_2 measurements were made in a separate cohort of control-state animals. The optical probe was placed in the left thalamus using a stereotactic surgical apparatus and pO_2 measurements were recorded during alternate free breathing of pure O_2, the hypoxic gas, and carbogen. The order in which gas compositions was administered was randomized amongst animals (n = 4). For each breathing gas condition, oxygen partial pressure data were digitally recorded until the measured pO_2 remained within a margin of ±10% for three minutes.

Discernment of radiation-induced necrosis vs. tumor

The utility of breathing gas modulations coupled with R_1 measurements for distinguishing radiation-induced necrosis from tumor was examined in cohorts of nine-week-old female BALB/c mice that were either: (i) exposed to a single 50-Gy (50% isodose) dose of single-hemispheric radiation (n = 6) using a Leksell Gamma Knife® Perfexion™ (Elekta; Stockholm, Sweden), or (ii) implanted with mouse Delayed Brain Tumor (DBT) glioma

cells (n = 7), or (iii) left as control-state (n = 4). Care was taken to coordinate similar tumor inoculation and irradiation sites.

Radiation Necrosis Model (32,33)—Mice were anesthetized with a ketamine/xylazine cocktail (intraperitoneal injection), restrained in a custom-made holder that attaches to the stereotactic frame of the Gamma Knife, and exposed to radiation focused to a ~1.33 mm^3 volume located 2.5 mm posterior and 2 mm to the left of bregma and 1.5 mm below the cortical surface. Late-onset radiation necrosis was allowed to develop for 13 weeks before the breathing gas/MRI experiment was performed.

Glioma Model (35)—Mice were secured in a stereotactic frame and anesthetized with isoflurane. DBT cells (~10,000) were injected over 10 minutes at a location 2 mm posterior and 2 mm to the left of bregma and 2 mm below the cortical surface. Tumors were allowed to grow for two weeks before the breathing gas/MRI experiment was performed.

R_1 data were collected (see *MRI methods*) on mice with radiation injury, mice with tumors, and control mice during alternate free breathing of: (i) carbogen and (ii) gas having a hypoxic composition (12.5% O_2). The order of gas administration was randomized amongst animals. R_1 data were collected 20 minutes after the start of free breathing of each gas to allow tissue oxygenation to reach equilibrium.

MRI Protocols

All MRI data were collected on a 4.7-T small-animal MRI system (Agilent Technologies, Santa Clara, CA) using a laboratory-built, actively decoupled, volume-transmit/surface-receive coil configuration. Mice were anesthetized with 0.8% isoflurane and restrained in a three-point head holder. Respiration was monitored throughout the experiment to ensure that animals maintained a ~100 breath per minute respiration rate. Anesthesia dosage was modulated, as necessary, to maintain a free-breathing rate of 100 breaths per minute. Highly evolution-time-resolved pure inversion-recovery ($\pi - \tau - \pi/2$ pulse sequence) R_1 data were collected during free breathing of each of the breathing gases (described above). R_1 data were collected using a single-slice (covering the thalamus ROI), fast-spin-echo pulse sequence with a non-slice-selective inversion pulse (to mitigate confounding apparent R_1 changes due to blood flow) and 32 linearly-spaced inversion times, ranging from 0.005 sec to 4.5 sec. Other imaging parameters were TE/TR = 20/5000 ms, echo train length = 8, FOV = 15×15 mm^2, slice thickness = 1 mm, matrix size = 64×64, averages = 1, dummy scans = 2, acquisition time = 20 min. and 20 sec. A T_2-weighted, spin-echo image was acquired between R_1 datasets, while tissue oxygenation equilibrated to the new gas condition, with parameters TE/TR = 50/1500 ms, FOV = 15×15 mm^2, slice thickness = 1 mm, matrix size = 128×128, averages = 4, acquisition time = 12 min. and 48 sec. Accounting for acquisition time of three R_1 maps (one for each breathing gas condition) and tissue pO_2 equilibration times after modulation of breathing gas (20 minutes), the total MRI experiment time was ~1 hr. 40 min.

Data analysis and statistics

Relaxation data were modeled as mono-exponential using Bayesian Probability Theory-based methods developed in our laboratory. (A toolbox of Bayesian-based, data-analysis programs is available for free download at http://bayesiananalysis.wustl.edu/.) Regions of interest (ROIs) were defined manually in ImageJ. Group statistical comparisons were calculated in MATLAB (The Mathworks, Natick, MA) first using analysis of variance (ANOVA) to test whether group means were significantly different, followed by Bonferroni's multiple comparisons to test for differences between specific groups. Intra-group comparisons of conditions (e.g., breathing of the hypoxic gas *vs.* carbogen in tumor-bearing mice) were conducted using paired two-tailed Student's t-tests. Relaxivity was calculated using a Bayesian Probability Theory-based Errors in Variables calculation (36). Unless noted otherwise, group data are reported as mean ± standard deviation.

RESULTS

Tissue water ^{1}H longitudinal relaxation rate constants (R_1) were measured at 4.7 Tesla in the brains of control-state mice (n = 4) during alternate free breathing of the hypoxic gas, pure oxygen, and carbogen. Global (voxel-wise averaged single slice) brain R_1 values were 0.74 ± 0.02 s^{-1}, 0.77 ± 0.03 s^{-1}, and 0.81 ± 0.02 s^{-1}, respectively (Fig. 1A, lower). The global brain R_1 during free breathing of carbogen was significantly different from R_1 during free breathing of either pure oxygen ($p < 0.05$) or the hypoxic gas ($p < 0.01$). R_1-maps (Fig. 1A, upper) show brain-tissue structure-specific R_1 differences under each of the three breathing-gas conditions.

The relationship between R_1 and tissue pO_2 was established by performing the same breathing gas experiment with an oxygen-sensitive optical probe implanted in the left thalamus of four control-state mice. Optical pO_2 measurements (Fig. 1B) and R_1 measurements trended similarly with modulation of breathing gas. Low (12 ± 5 mmHg), moderate (66 ± 11 mmHg), and high (88 ± 7 mmHg) pO_2 values were observed during alternate free breathing of the hypoxic gas composition, pure O_2, and carbogen, respectively. The pO_2 values for each breathing gas condition were significantly different from one another: $p < 0.01$ for pure O_2 *vs.* hypoxic gas and carbogen versus hypoxic gas, and $p < 0.05$ for pure O_2 *vs.* carbogen. From these data, and ROI measures of R_1 in comparable brain regions, we calculated the *in vivo* relaxivity (r_1) of oxygen in control-state brain tissue to be $9\times10^{-4} \pm 3\times10^{-4}$ $mmHg^{-1}s^{-1}$ or, equivalently, 0.64 ± 0.21 $mM^{-1}s^{-1}$. (Fig. 1C).

In control-state mice, the greatest difference in tissue oxygenation (and thus R_1) was observed between breathing carbogen *vs.* the hypoxic gas. This breathing gas experiment was applied under these two conditions in mouse models of single-hemisphere, radiation-induced necrosis and glioma. Tumor and radiation necrosis lesions showed contrast *vs.* surrounding tissue in R_1-maps acquired during both breathing gas conditions (Fig. 2B–C, F–G). Qualitatively, the lesions were more conspicuous in the R_1-maps than in corresponding T_2-weighted images (Fig. 2A,E). Differences in R_1 between each breathing-gas condition were resolvable in R_1-maps acquired from mice with radiation necrosis (Fig. 2F–G) and control-state mice (Fig. 2J–K), but not in tumor-bearing mice (Fig. 2B–C). Lesion-specific R_1 histograms revealed a shift in R_1 in the cortex of control-state subjects when the

breathing gas was modulated (Fig. 2L). A smaller breathing-gas-induced shift in R_1 was observed in radiation necrosis lesions (Fig. 2H), while no shift in R_1 was observed in tumors (Fig. 2D). Quantitatively, R_1 changed significantly when the breathing gas was modulated between carbogen and the hypoxic gas composition in ROIs encompassing radiation necrosis lesions and comparable regions of cortex in control-state mice ($p < 0.03$) but not, interestingly, in tumor (Fig. 3A). Lesion-specific R_1 under either breathing gas condition alone distinguished the two pathologies ($p < 0.05$). Lesion-specific change in R_1 due to breathing gas modulation (ΔR_1) distinguished the two pathologies with greater statistical power ($p < 0.01$): $0.01 \pm 0.02\ s^{-1}$ in tumor, $0.05 \pm 0.01\ s^{-1}$ in radiation necrosis lesions, and $0.07 \pm 0.01\ s^{-1}$ in cortex from control-state mice (Fig. 3B). Compared to R_1 and mmHg measures alone, ΔR_1 measurements were better able to distinguish radiation-induced lesions from tumor lesions.

DISCUSSION

Brain tissue water ^1H longitudinal relaxation rate constants (R_1) are sensitive to dissolved diatomic (molecular) oxygen. The free breathing of pure oxygen *vs.* a hypoxic gas *vs.* carbogen generates moderate, low, and high R_1, respectively, in control-state mice. Optical-based tissue pO_2 measurements corroborate the direct relationship between R_1 and tissue oxygenation (Fig. 1, Eq. 1). Our findings are in accordance with previous MRI-based studies from other laboratories in which the paramagnetic nature of molecular oxygen was exploited to make MRI-based, quantitative inferences concerning tissue oxygenation (1–10). From the linear relationship of pO_2 *vs.* R_1, we calculate the relaxivity of O_2 in brain tissue to be 8.5 $mmHg^{-1}s^{-1}$ or, equivalently, 0.6 $mM^{-1}s^1$.

Non-invasive discrimination of post-treatment radiation necrosis from recurrent tumor remains a significant clinical challenge. Lesion R_1 ($p < 0.05$) and ΔR_1 ($p < 0.01$) distinguish radiation necrosis, tumor, and brain tissue of control-state rodent subjects. The O_2-driven ΔR_1 measurements are more robust in making this distinction. The O_2-sensitive ΔR_1 methodology can, in principle, be readily extended to the clinic, where breathing gas challenges have been well tolerated (3,7,26,30,37–40). Further work, in animal models and subsequently in humans, is necessary to show that R_1 and/or ΔR_1 measurements can discriminate between radiation necrosis and tumor *in the same brain*. Still, it is encouraging that O_2-sensitive ΔR_1 in tumor compares well to recent studies by Khan, et al. (41) (an electron spin resonance study), and Hallac, et al. (29) (a MRI-based study), which show similar small changes in absolute tumor pO_2 and R_1 relative to normal contralateral brain during modulation of breathing gas between room air and carbogen.

Breathing carbogen is known to increase blood flow in the brain, which could confound inferences about tissue oxygenation from R_1 measurements. An inversion-recovery experiment to measure R_1, such as that used in this work, involves perturbation of spins from their equilibrium state and subsequent monitoring of their return to thermal equilibrium. The measured return to equilibrium, characterized by R_1, will appear artificially rapid if unperturbed spins flow into the imaging plane during the experiment. In this study, we have minimized these flow effects by using a non-slice-selective, adiabatic inversion radio-frequency pulse that equally perturbs all spins in the sample, independent of location.

In conclusion, because the longitudinal relaxation rate constant of tissue water is linearly dependent upon tissue oxygenation, MRI-based R_1 measurements can directly and quantitatively map changes in tissue O_2 concentration. We have reported herein the *in vivo* (mouse brain) pO_2 relaxivity at 4.7 Tesla. Further, we have shown that radiation necrosis and tumor in mouse models can be distinguished using oxygen-sensitive MRI mapping. This noninvasive, MRI-based measurement of tissue O_2 holds promise for translation to the clinic.

REFERENCES

1. Winter JD, Estrada M, Cheng H-LM. Normal Tissue Quantitative T1 and T2 MRI Relaxation Time Responses to Hypercapnic and Hyperoxic Gases. Acad Radiol. 2011; 18:1159–1167. doi: 10.1016/j.acra.2011.04.016. [PubMed: 21704536]
2. Zhang Z, Hallac RR, Peschke P, Mason RP. A noninvasive tumor oxygenation imaging strategy using magnetic resonance imaging of endogenous blood and tissue water. Magn Reson Med. 2013 doi: 10.1002/mrm.24691.
3. Remmele S, Sprinkart AM, Müller A, et al. Dynamic and simultaneous MR measurement of R1 and R2* changes during respiratory challenges for the assessment of blood and tissue oxygenation. Magn Reson Med. 2013; 70:136–146. doi: 10.1002/mrm.24458. [PubMed: 22926895]
4. Mason RP, Rodbumrung W, Antich PP. Hexafluorobenzene: a Sensitive 19F NMR Indicator of Tumor Oxygenation. NMR Biomed. 1996; 9:125–134. doi: 10.1002/(SICI)1099-1492(199605)9:3<125::AID-NBM405>3.0.CO;2-F. [PubMed: 8892399]
5. Jordan BF, Magat J, Colliez F, et al. Mapping of oxygen by imaging lipids relaxation enhancement: A potential sensitive endogenous MRI contrast to map variations in tissue oxygenation. Magn Reson Med. 2013; 70:732–744. doi: 10.1002/mrm.24511. [PubMed: 23023932]
6. Mason RP, Antich PP, Babcock EE, Constantinescu A, Peschke P, Hahn EW. Non-invasive determination of tumor oxygen tension and local variation with growth. Int J Radiat Oncol. 1994; 29:95–103. doi: 10.1016/0360-3016(94)90231-3.
7. O'Connor JPB, Jackson A, Buonaccorsi GA, et al. Organ-specific effects of oxygen and carbogen gas inhalation on tissue longitudinal relaxation times. Magn Reson Med. 2007; 58:490–496. doi: 10.1002/mrm.21357. [PubMed: 17763345]
8. O'Connor JPB, Naish JH, Parker GJM, et al. Preliminary Study of Oxygen-Enhanced Longitudinal Relaxation in MRI: A Potential Novel Biomarker of Oxygenation Changes in Solid Tumors. Int J Radiat Oncol. 2009; 75:1209–1215. doi: 10.1016/j.ijrobp.2008.12.040.
9. Kodibagkar VD, Wang X, Pacheco-Torres J, Gulaka P, Mason RP. Proton imaging of siloxanes to map tissue oxygenation levels (PISTOL): a tool for quantitative tissue oximetry. NMR Biomed. 2008; 21:899–907. doi: 10.1002/nbm.1279. [PubMed: 18574806]
10. Zhao D, Ran S, Constantinescu A, Hahn EW, Mason RP. Tumor Oxygen Dynamics: Correlation of In Vivo MRI with Histological Findings. Neoplasia. 2003; 5:308–318. doi: 10.1016/S1476-5586(03)80024-6. [PubMed: 14511402]
11. Padhani AR. Where are we with imaging oxygenation in human tumours? Cancer Imaging. 2005; 5:128–130. doi: 10.1102/1470-7330.2005.0103. [PubMed: 16321774]
12. Krause B, Beck R, Souvatzoglou M, Piert M. PET and PET/CT studies of tumor tissue oxygenation. Q J Nucl Med Mol Imaging. 2006; 50:28–43. [PubMed: 16557202]
13. Bourgeois M, Rajerison H, Guerard F, Mougin-Degraef M, Barbet J, Michel N, Cherel M, Faivre-Chauvet A. Contribution of [64Cu]-ATSM PET in molecular imaging of tumour hypoxia compared to classical [18F]-MISO--a selected review. Nucl Med Rev. Cent East Eur. 2011; 14:90–95. [PubMed: 22219149]
14. He X, Yablonskiy DA. Quantitative BOLD: Mapping of human cerebral deoxygenated blood volume and oxygen extraction fraction: Default state. Magn Reson Med. 2007; 57:115–126. doi: 10.1002/mrm.21108. [PubMed: 17191227]
15. An H, Lin W. Quantitative Measurements of Cerebral Blood Oxygen Saturation Using Magnetic Resonance Imaging. J. Cereb. Blood Flow Metab. 2000; 20:1225–1236. [PubMed: 10950383]

16. He X, Zhu M, Yablonskiy DA. Validation of oxygen extraction fraction measurement by qBOLD technique. Magn Reson Med. 2008; 60:882–888. doi: 10.1002/mrm.21719. [PubMed: 18816808]
17. Ogawa S, Lee TM, Kay AR, Tank DW. Brain magnetic resonance imaging with contrast dependent on blood oxygenation. Proc Nat Acad Sci. 1990; 87:9868–9872. [PubMed: 2124706]
18. Christen T, Lemasson B, Pannetier N, Farion R, Segebarth C, Rémy C, Barbier EL. Evaluation of a quantitative blood oxygenation level-dependent (qBOLD) approach to map local blood oxygen saturation. NMR Biomed. 2011; 24:393–403. doi: 10.1002/nbm.1603. [PubMed: 20960585]
19. Ogawa S, Menon RS, Tank DW, Kim SG, Merkle H, Ellermann JM, Ugurbil K. Functional brain mapping by blood oxygenation level-dependent contrast magnetic resonance imaging. A comparison of signal characteristics with a biophysical model. Biophys J. 1993; 64:803–812. doi: 10.1016/S0006-3495(93)81441-3. [PubMed: 8386018]
20. Christen T, Lemasson B, Pannetier N, Farion R, Remy C, Zaharchuk G, Barbier EL. Is T2* Enough to Assess Oxygenation? Quantitative Blood Oxygen Level–Dependent Analysis in Brain Tumor. Radiology. 2012; 262:495–502. [PubMed: 22156990]
21. Howe FA, Robinson SP, McIntyre DJ, Stubbs M, Griffiths JR. Issues in flow and oxygenation dependent contrast (FLOOD) imaging of tumours. NMR Biomed. 2001; 14:497–506. [PubMed: 11746943]
22. Chiarotti G, Cristiani G, Giulotto L. Proton relaxation in pure liquids and in liquids containing paramagnetic gases in solution. Il Nuovo Cimento. 1955; 1:863–873. doi: 10.1007/BF02731333.
23. Lai C-S, Stair SJ, Miziorko H, Hyde JS. Effect of oxygen and the lipid spin label TEMPO-laurate on fluorine-19 and proton relaxation rates of the perfluorochemical blood substitute, FC-43 emulsion. J Magn Reson. 1984; 57:447–452. 1969. doi: 10.1016/0022-2364(84)90259-2.
24. D' Othée BJ, Rachmuth G, Munasinghe J, Lang EV. The effect of hyperoxygenation on T1 relaxation time in vitro1. Acad Radiol. 2003; 10:854–860. doi: 10.1016/S1076-6332(03)00004-7. [PubMed: 12945919]
25. Zaharchuk G, Martin AJ, Rosenthal G, Manley GT, Dillon WP. Measurement of cerebrospinal fluid oxygen partial pressure in humans using MRI. Magn Reson Med. 2005; 54:113–121. doi: 10.1002/mrm.20546. [PubMed: 15968660]
26. Berkowitz BA, McDonald C, Ito Y, Tofts PS, Latif Z, Gross J. Measuring the human retinal oxygenation response to a hyperoxic challenge using MRI: Eliminating blinking artifacts and demonstrating proof of concept. Magn Reson Med. 2001; 46:412–416. [PubMed: 11477648]
27. Matsumoto K, Bernardo M, Subramanian S, Choyke P, Mitchell JB, Krishna MC, Lizak MJ. MR assessment of changes of tumor in response to hyperbaric oxygen treatment. Magn Reson Med. 2006; 56:240–246. doi: 10.1002/mrm.20961. [PubMed: 16795082]
28. Nestle N, Baumann T, Niessner R. Oxygen determination in oxygen-supersaturated drinking waters by NMR relaxometry. Water Res. 2003; 37:3361–3366. doi: 10.1016/S0043-1354(03)00211-2. [PubMed: 12834729]
29. Hallac RR, Zhou H, Pidikiti R, Song K, Stojadinovic S, Zhao D, Solberg T, Peschke P, Mason RP. Correlations of noninvasive BOLD and TOLD MRI with pO2 and relevance to tumor radiation response. Magn Reson Med. 2014; 71:1863–1873. doi: 10.1002/mrm.24846. [PubMed: 23813468]
30. Ding Y, Mason RP, McColl RW, Yuan Q, Hallac RR, Sims RD, Weatherall PT. Simultaneous measurement of tissue oxygen level-dependent (TOLD) and blood oxygenation level-dependent (BOLD) effects in abdominal tissue oxygenation level studies. J Magn Reson Imaging. 2013; 38:1230–1236. doi: 10.1002/jmri.24006. [PubMed: 23749420]
31. Tatum JL. Hypoxia: Importance in tumor biology, noninvasive measurement by imaging, and value of its measurement in the management of cancer therapy. Int J Radiat Biol. 2006; 82:699–757. doi: 10.1080/09553000601002324. [PubMed: 17118889]
32. Jiang X, Engelbach JA, Yuan L, et al. Anti-VEGF Antibodies Mitigate the Development of Radiation Necrosis in Mouse Brain. Clin Cancer Res. 2014; 20:2695–2702. doi: 10.1158/1078-0432.CCR-13-1941. [PubMed: 24647570]
33. Jiang X, Perez-Torres CJ, Thotala D, et al. A GSK-3β Inhibitor Protects Against Radiation Necrosis in Mouse Brain. Int J Radiat Oncol. 2014; 89:714–721. doi: 10.1016/j.ijrobp.2014.04.018.

34. Kumar AJ, Leeds NE, Fuller GN, Van Tassel P, Maor MH, Sawaya RE, Levin VA. Malignant Gliomas: MR Imaging Spectrum of Radiation Therapy- and Chemotherapy-induced Necrosis of the Brain after Treatment. Radiology. 2000; 217:377–384. doi: 10.1148/radiology.217.2.r00nv36377. [PubMed: 11058631]

35. Kumanishi T. Brain tumors induced with Rous sarcoma virus, Schmidt-Ruppin strain. I. Induction of brain tumors in adult mice with Rous chicken sarcoma cells. Jpn J Exp Med. 1967; 37:461–474. [PubMed: 4301953]

36. Linden, W von der; Dose, V.; Toussaint, U von. Bayesian Probability Theory: Applications in the Physical Sciences. Cambridge University Press; 2014.

37. Taylor NJ, Baddeley H, Goodchild KA, et al. BOLD MRI of human tumor oxygenation during carbogen breathing. J Magn Reson Imaging. 2001; 14:156–163. doi: 10.1002/jmri.1166. [PubMed: 11477674]

38. Alonzi R, Padhani AR, Maxwell RJ, Taylor NJ, Stirling JJ, Wilson JI, d'Arcy JA, Collins DJ, Saunders MI, Hoskin PJ. Carbogen breathing increases prostate cancer oxygenation: a translational MRI study in murine xenografts and humans. Br J Cancer. 2009; 100:644–648. [PubMed: 19190629]

39. Powell MEB, Hill SA, Saunders MI, Hoskin PJ, Chaplin DJ. Effect of carbogen breathing on tumour microregional blood flow in humans. Radiother Oncol. 1996; 41:225–231. doi: 10.1016/S0167-8140(96)01833-6. [PubMed: 9027938]

40. Powell MEB, Hill SA, Saunders MI, Hoskin PJ, Chaplin DJ. Human Tumor Blood Flow Is Enhanced by Nicotinamide and Carbogen Breathing. Cancer Res. 1997; 57:5261–5264. [PubMed: 9393746]

41. Khan N, Williams BB, Hou H, Li H, Swartz HM. Repetitive Tissue pO2 Measurements by Electron Paramagnetic Resonance Oximetry: Current Status and Future Potential for Experimental and Clinical Studies. Antioxid Redox Signal. 2007; 9:1169–1182. doi: 10.1089/ars.2007.1635. [PubMed: 17536960]

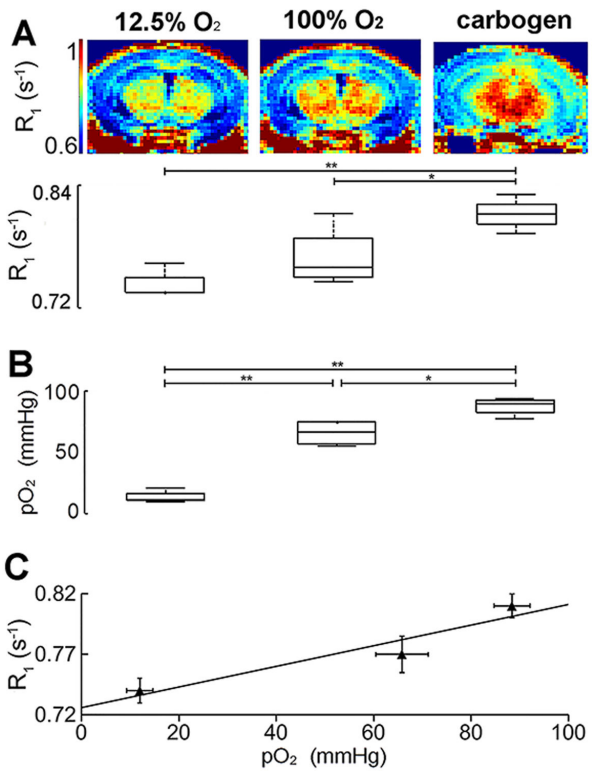

Figure 1.

Representative R_1 maps and group whole-brain R_1 measurements (A), group optical probe pO_2 measurements (B), and relaxivity calculations (C) made in the brains of control-state mice (n = 4) during free breathing of a hypoxic gas (first column), pure oxygen (second column), and carbogen (third column). Representative R_1-maps illustrate R_1 differences between breathing gas conditions (A). Whole-brain R_1 values were low (0.74±0.02 s^{-1}) during free breathing of the hypoxic gas, moderate (0.77±0.03 s^{-1}) during free breathing of pure O_2, and high (0.81±0.02 s^{-1}) during free breathing of carbogen (A). R_1 measurements made during free breathing of carbogen were significantly different from those made during free breathing of pure oxygen and the hypoxic gas. Optical measurements support the *in vivo* R_1 measurements: Low (12 ± 5 mmHg), moderate (66 ± 11 mmHg), and high (88 ± 7 mmHg) pO_2 values were observed during free breathing of the hypoxic gas composition, pure O_2, and carbogen, respectively. The pO_2 values for each breathing gas condition were significantly different from each other. From these data, the relaxivity (r_1) of oxygen in control-state brain tissue was calculated to be $9\times10^{-4} \pm 3\times10^{-4}$ $mmHg^{-1}s^{-1}$ or, equivalently, 0.64 ± 0.21 $mM^{-1}s^{-1}$. $p < 0.05$, denoted by * and $p < 0.01$, denoted by **.

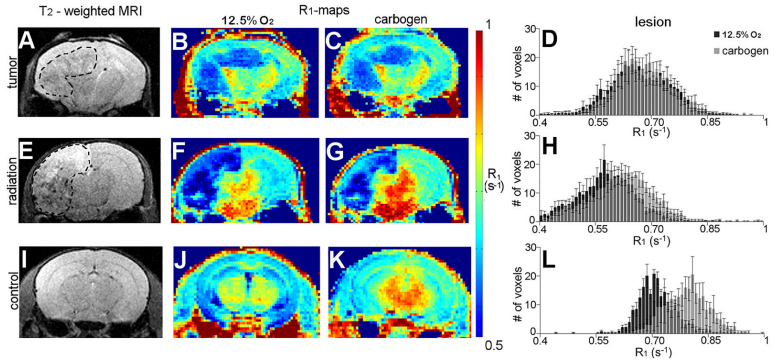

Figure 2.

Representative T_2-weighted images (A,E,I), R_1-maps (B–C, F–G, J–K), and R_1-histograms (D,H,L) from mice with tumors, mice with radiation necrosis, and untreated control-state mice during alternate free breathing of the hypoxic gas and carbogen. Tumor and radiation necrosis lesions are conspicuous in R_1-maps acquired during both breathing gas conditions (B–C, F–G). Qualitatively, these lesions are more obvious in R_1-maps than in standard T_2-weighted images (A,E), where lesions are delineated with a dashed line for clarity. The differences in R_1 between breathing gas conditions are evident in R_1-maps acquired from mice with radiation necrosis (F–G) and control-state mice (j–K), but not in tumor-bearing mice (B–C). A broad, oxygen-induced shift in voxel-wise R_1 values in control-state cortex was observed in lesion-specific histograms (Fig. 3L). A smaller shift in voxel-wise R_1 values was observed in radiation necrosis lesions (Fig. 3H). No shift in voxel-wise R_1 was observed in tumor lesions (Fig. 3D).

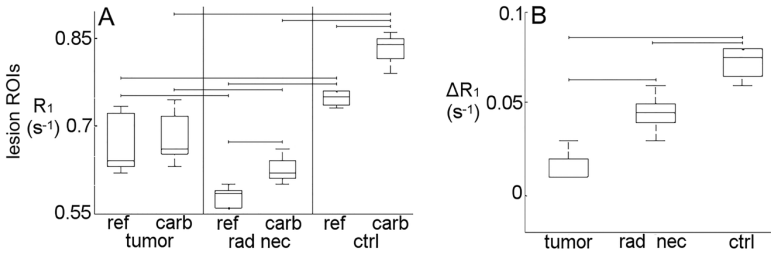

Figure 3.

Breathing gas modulation experiments applied in animal models of radiation necrosis (n = 6) and glioma (n = 7) and control-state animals (n = 4) using carbogen and the hypoxic gas. Lesion-specific R_1 changed significantly in radiation necrosis lesions and in comparable region of cortex in control-state mice when breathing gas was modulated between carbogen and the hypoxic gas ($p < 0.05$), but not in tumor tissue (A). Lesion-specific changes in R_1 due to breathing gas modulation (ΔR_1) were calculated to be $0.01 \pm 0.02\ s^{-1}$ (i.e., no change) for tumor, $0.05 \pm 0.01\ s^{-1}$ for cortex with radiation necrosis, and $0.07 \pm 0.01\ s^{-1}$ for control-state cortex. Lesion-specific ΔR_1 differentiated between radiation necrosis and tumor-bearing groups ($p < 0.01$, B). Lesion R_1 during breathing of either the reference gas or carbogen alone also distinguished between groups ($p < 0.05$). Brackets indicate $p < 0.05$.